

AD-A104 424

DEFENCE RESEARCH ESTABLISHMENT VALCARTIER (QUEBEC)
DETERMINATION OF PULSED CO₂ LASER DAMAGE THRESHOLDS OF OPTICAL --ETC(U)
MAR 81 J C ANSTIL, R W MACPHERSON

F/6 20/6

UNCLASSIFIED DREV-R-4197/81

ML

1 OF 1
A
10024.0

END
DATE
FEBRUARY
NO. 81
DTIC

AD A 104 424

NON CLASSIFIED
UNCLASSIFIED//CONFIDENTIAL

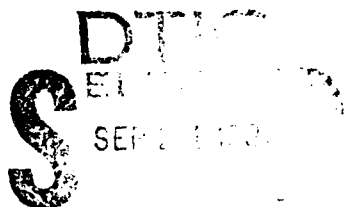
3

NON CLASSIFIED
UNCLASSIFIED//CONFIDENTIAL
UNCLASSIFIED//CONFIDENTIAL

DETERMINATION OF PULSED CO₂ LASER
DAMAGE THRESHOLDS OF OPTICAL SURFACES

J.C. Van Ooij

R.W. MacPherson



DRC FILE COPY

Centre de Recherches pour la Défense
Defence Research Establishment
Valcartier, Québec

BUREAU - RECHERCHE ET DEVELOPPEMENT
MINISTÈRE DE LA DEFENSE NATIONALE
CANADA

NON CLASSIFIED
DIFFUSION AUTORISÉE

RESEARCH AND DEVELOPMENT BRANCH
DEPARTMENT OF NATIONAL DEFENCE
CANADA

CRDV R-4197/81
DOSSIER: 3633B-039

UNCLASSIFIED

DREV-R-4197/81
FILE: 3633B-039

DETERMINATION OF PULSED CO₂ LASER
DAMAGE THRESHOLDS OF OPTICAL SURFACES

by

J.C. Anctil and R.W. MacPherson

CENTRE DE RECHERCHES POUR LA DEFENSE
DEFENCE RESEARCH ESTABLISHMENT
VALCARTIER
TEL: (418) 844-4271

Québec, Canada

March/mars 1981

NON CLASSIFIÉ

111745

B

UNCLASSIFIED

i

RESUME

Nous décrivons une technique expérimentale permettant de déterminer le seuil d'endommagement des surfaces optiques de verre et de plastique irradiées par un laser CO₂ TEA impulsif. Les densités d'énergie correspondant à une probabilité d'endommagement de 50%, telles qu'estimées par une analyse probit, sont de 4.0 J/cm² pour la silice fondue, de 2.1 J/cm² pour le verre sodocalcique, de 2.3 J/cm² pour le thermoplastique, de 2.3 J/cm² pour le plastique acrylique et de 1.7 J/cm² pour le polystyrène. Nous présentons une interprétation des distributions statistiques observées en fonction de divers mécanismes d'endommagement. Enfin, plusieurs améliorations susceptibles d'accroître la précision des résultats obtenus sont suggérées. (NC)

ABSTRACT

An experimental technique is described for determining the damage thresholds of glass and plastic optical material surfaces, opaque to laser radiations, when irradiated with a pulsed TEA-CO₂ laser. Use of a probit analysis to estimate the irradiance required for a 50% probability of damage gives threshold levels of 4.0 J/cm² for fused silica, 2.1 J/cm² for soda-lime glass, 2.3 J/cm² for polycarbonate, 2.3 J/cm² for acrylic and 1.7 J/cm² for polystyrene plastics. The significance of the statistical distributions observed in attributing various mechanisms to the damage is discussed. Finally, some improvements are suggested to make the measurements more accurate! (U)

Accession No.	
RTT:	CH 101
PLAT:	
U.S.A.:	

A

UNCLASSIFIED

ii

TABLE OF CONTENTS

RESUME/ABSTRACT	i
1.0 INTRODUCTION	1
2.0 EXPERIMENTAL	2
2.1 Damage Testing Facility	2
2.2 Procedure	5
3.0 STATISTICAL ANALYSIS OF DAMAGE MEASUREMENTS	14
3.1 Sources of Statistics in Threshold Measurements	14
3.2 Probit Analysis	15
4.0 RESULTS AND DISCUSSION	17
5.0 CONCLUSION	25
6.0 ACKNOWLEDGEMENTS	26
7.0 REFERENCES.	27
TABLE I	
FIGURES 1 to 12	
APPENDIX A: Maximum Likelihood Estimation by the Probit Method	29

UNCLASSIFIED

1

1.0 INTRODUCTION

A number of workers have shown that damage to transparent optical materials from laser radiation is a statistical phenomenon. Bass and Barret (Ref. 1) first demonstrated the statistical nature of the damage due to an intrinsic electron avalanche breakdown, while others (Refs. 2-5) showed that damage due to absorbing inclusions and structural defects in the material were also statistical. In these cases, the concept of a damage threshold could only be defined statistically since irradiating apparently identical sites with identical laser pulses produced damage for some of the trials only.

On the other hand, homogeneous absorption by the irradiated material is non statistical, and materials damaged by this phenomenon should show a definite threshold. Under this assumption, the absence or presence of statistics could be an indication of the damaging mechanism. Caution is required, however, since there are many sources of statistical fluctuations associated to damage threshold experiments. For example, lasers' inherent pulse-to-pulse variation in energy may mask the statistics of the damage phenomenon; the surface conditions of the samples may influence the amount of energy absorbed; the actual failure mechanism, triggered by the absorbed radiation, may be statistical even if the absorption is not.

In this work, we present some typical results of damage experiments on various glasses and plastics, opaque to the laser radiation. Damage is defined on the basis of changes which occur in the physical appearance of the surface of the materials. Since the absorption is homogeneous in the materials chosen, the damage is presumed to be non-statistical.

UNCLASSIFIED

2

To measure distributions in the damage thresholds, we adapted the experimental technique used by Hacker and Halverson (Ref. 6) for determining the breakdown threshold of gases. The influence of laser energy fluctuations is largely eliminated by recording the energy of each pulse along with an indication of whether or not damage occurred. Any remaining statistics that can be attributed to the damage phenomenon may be used to characterize its process.

Section 2 describes the experimental setup and the procedure for acquiring the data. An outline of the statistical analysis which allows to estimate the damage threshold and the parameters of the probability density function appears in Section 3. The results and a discussion of their significance follow in Section 4.

This work was performed at DREV, between January 1977 and May 1980, as partial fulfilment of tasking for DLAEEM under PCN 33B39, Laser Induced Damage to Optical Surfaces.

2.0 EXPERIMENTAL

2.1 Damage Testing Facility

Figure 1 schematically illustrates the physical setup used for the damage tests. Damage was induced by a Laflamme type (Ref. 7) TEA-CO₂ laser (Ref. 8) modified for variable pulse length operation (Ref. 9). The pulse length of this laser can be varied from 0.1 μ s to 100 μ s (width at 10% maximum height) by changing the reflectivity of the output coupler and the composition of the gas mixture. Figure 2 shows the typical waveform of the 34- μ s pulses used in these experiments. The available pulse energy ranges from 5 to 50 J, depending on the pulse length and the discharge voltage. The laser operation is multimode on the P20 line, at 10.6 μ m, with a beam approximately 50 mm by 50 mm at the output.

UNCLASSIFIED

3

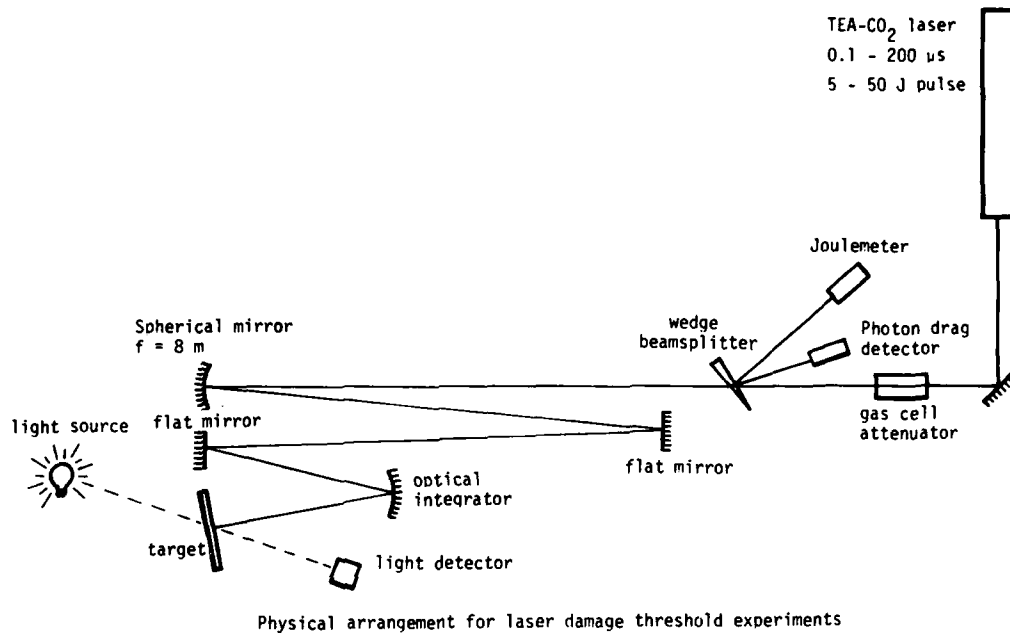


FIGURE 1 - Physical setup for laser damage threshold experiments. The pressure of propylene in the gas cell attenuator controls the beam energy. The two reflected beams from the NaCl, 5°-wedge beamsplitter are monitored by the pyroelectric Joulemeter for a measure of the beam energy, and by the photon drag detector for the time evolution of the laser pulse. The spherical mirror and the optical integrator produce a ~ 12 mm square spot on the target plane. Long-focal-length mirrors were used to avoid the possibility of air breakdowns in the focal regions. Except at the flat turning mirror, all angles between incident and reflected beams were kept less than 10° to reduce polarization effects at the surface of dielectrics, and aberrations from the spherical mirrors.

UNCLASSIFIED

4

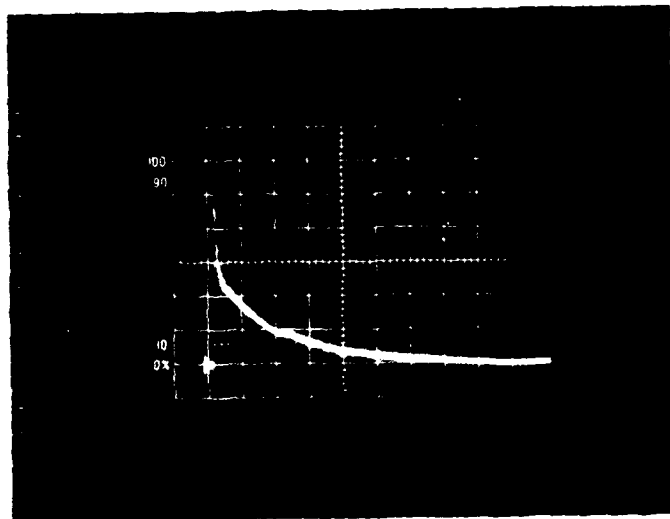


FIGURE 2 - Time evolution of the laser pulse recorded from a photon drag detector with a 150-MHz-bandwidth oscilloscope terminated with 50Ω . Pulse width of 34 μs is measured as the width at 10% of the maximum.

UNCLASSIFIED

5

A series of plane and spherical mirrors (Fig. 1) folded and focussed the beam to a spot approximately 12-mm square at the target plane. A homogenizing reflector, consisting of 32 small flat mirrors mounted on a spherical surface, was also incorporated to obtain a uniformly distributed beam profile. This arrangement avoided air breakdown, and allowed the use of small off-axis angles to reduce the effects of spherical aberrations. It also provided for spatial filtering if a more uniform beam profile were needed for greater precision in future experiments. The current profile at the target plane is flat to within 10%. Provision was made for a second NaCl, 5°-wedge beam splitter to be inserted between the final focussing mirror and the target plane to provide two additional sample beams, one for monitoring the laser wavelength by means of a CO₂ laser spectrum analyzer, the other for future continuous monitoring of the laser beam profile at the target plane with a pyroelectric vidicon camera.

A mechanism (Fig. 3) held the target and repositioned it between the shots to expose a fresh site to the laser beam. This mechanism allowed the laser beam to scan the target in raster fashion to cover rectangular samples from 5 cm to 30 cm on a side.

2.2 Procedure

The technique used was a multiple-shot, 1-on-1 experiment in which each site of the sample was irradiated once by a pulse from the CO₂ laser. This avoided cumulative effects, such as laser polishing or conditioning of the sample (Ref.10), and ensured that the effect of each shot was independent. To obtain as many damaging shots as undamaging ones, we controlled the laser energy from shot-to-shot with a gas cell attenuator. We attempted to collect sufficient data at each energy level to ensure at least one surviving or one damaged site.

UNCLASSIFIED

6

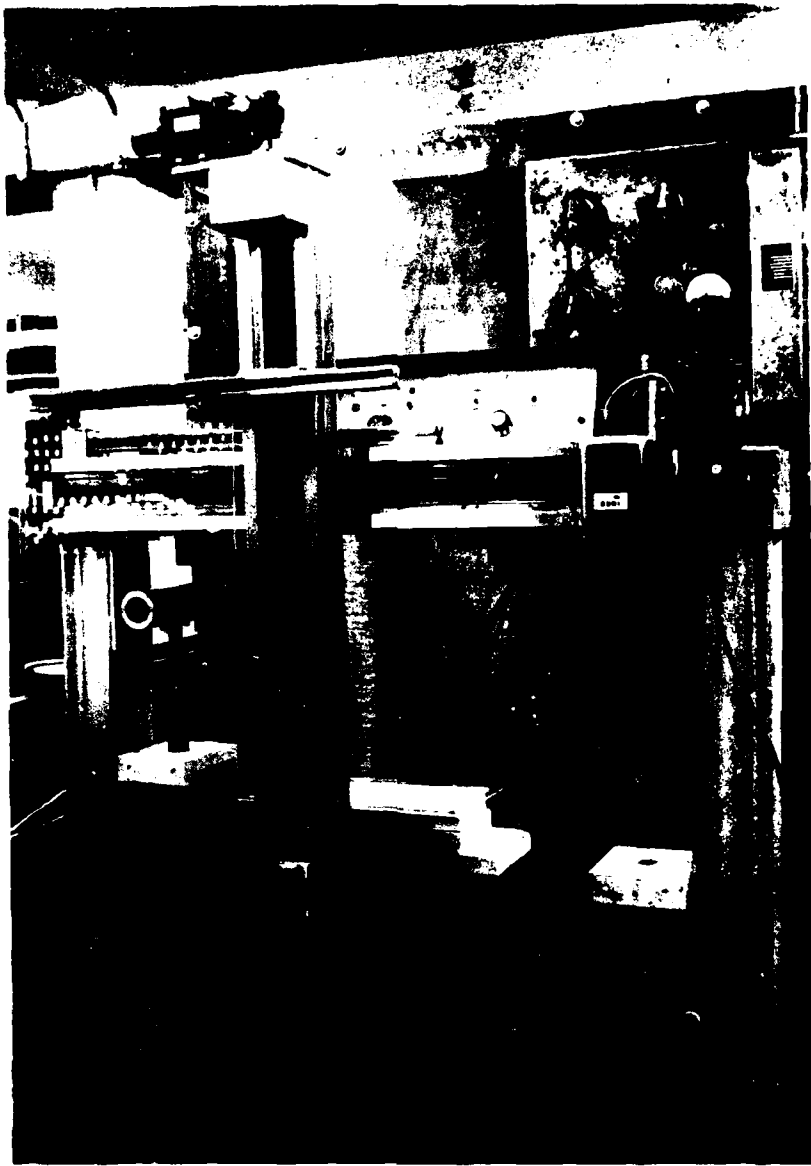


FIGURE 3 - Mechanical scanner used to transport a fresh sample site into position between laser shots. A 5 to 30 cm square sample may be accommodated; it moves horizontally between adjustable limits then shifts 20 mm vertically to start a new horizontal scan. Scan speed may be set over a wide range but, in this experiment it was adjusted to space sample sites ~20 mm apart between laser shots.

UNCLASSIFIED

7

The joulemeter produces a peak voltage pulse proportional to the laser beam energy it monitors. The corresponding energy actually falling on the target plane can be calculated if the ratio between the joulemeter voltage and the target energy is known. This ratio was obtained by direct measurement, and frequently verified so as to detect any variation caused by inadvertent changes in the alignment or the optical properties of the components.

To increase precision, we offset the joulemeter voltage by a known constant before reading its peak with a digitizer and storing it in one of two 256-channel memories. Short duration noise, which appears on the joulemeter cable at the time of the laser firing, prevents the use of the peak reading mode of the digitizer. However, since the joulemeter voltage rises slowly, over several milliseconds, and reaches its maximum after the noise has subsided, the reading could be taken by triggering the digitizer with a pulse delayed to coincide with the peak.

Damage was detected visually since all the sample materials were transparent in the visible region of the spectrum. The polystyrene, polycarbonate and silica surfaces were damaged by melting. Damage in these materials was detected by projecting images of their surfaces on a screen, with a white light, to observe their patterns. It appeared as white spots in the acrylic plastic (PMMA), and as fine cracks, which occurred within 5-10 s of irradiation, in the glass. In these two materials, damage was detected by illuminating the samples with a collimated beam of white light from an arc lamp and by viewing the laser irradiated area with a standard TV monitor.

UNCLASSIFIED

8

A 555 timer, connected as a bistable multivibrator, registered whether a site was damaged or not. When damage occurred, the multivibrator output was manually set high, otherwise, it was left low. The pulse that triggered the digitizer for the joulemeter also triggered a second digitizer which recorded the state of the multivibrator in the second 256-channel memory and reset it low. This allowed several seconds, after the laser shot, for the damage decision to be made. We must be aware that, although the energy of the n^{th} laser shot was recorded in the n^{th} channel of the first memory, the damage decision was recorded later in t , the $n+1^{\text{th}}$ channel of the second memory. This can easily be integrated to the computer program to perform the analysis.

Via a CRT terminal, the data computed from the numerous shots was transferred from the memories to DREV's main computer through a custom-built interface. Within a few seconds, preliminary results of the statistical analysis were displayed on the CRT terminal's screen (Figs. 4-8) so that one could rapidly determine if the data was adequate.

The samples were tested as received from the distributors. No special treatments were applied to the surfaces beforehand other than the removal of any obvious dirt and dust with compressed air. The soda-lime glass was ordinary window glass from the carpentry shop. The polycarbonate plastic sheet was Lexan^{R*} 9030, the acrylic plastic was Plexiglas^{TM**}, and the polystyrene was a "K-LUX" Safe-t-vue clear sheet. The silica was a Corning 7940 fused-silica plate with a commercial polish.

* R Trademark of the General Electric Company, Pittsfield, Mass. 01201

** TM Trademark of the Rohm and Hass Co., Philadelphia Pa. 19105

UNCLASSIFIED

9

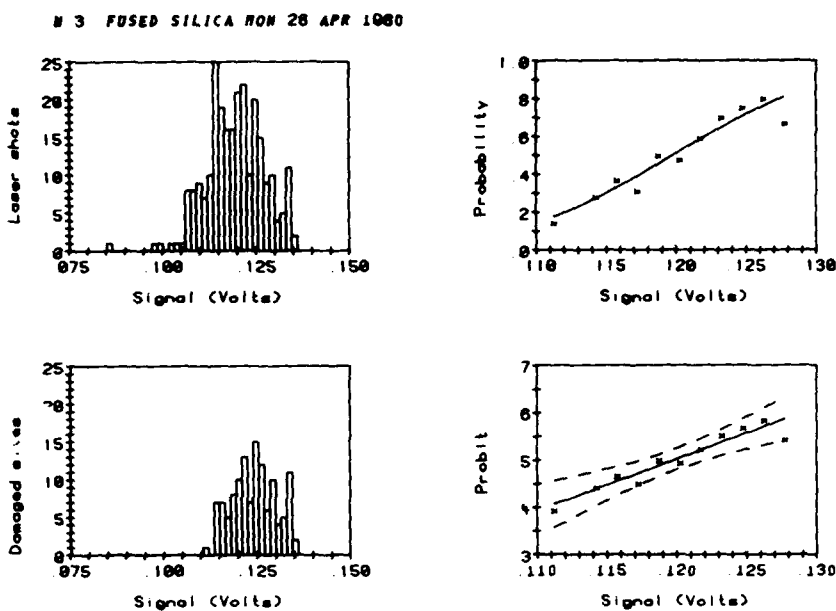


FIGURE 4 - Experimental results for the measurement of the damage threshold of fused silica irradiated by a 34- μ s-long TEA-CO₂ laser pulse at 10.6 μ m. The upper left graph is a histogram of all laser shots as a function of laser energy (represented by the signal voltage from the energy meter). The lower left graph is a histogram of those shots which damaged the surface. (In fused silica, the damage was characterized by the onset of surface melting). The upper right graph shows the probability of causing damage as a function of laser energy. The crosses represent the relative frequencies of damage obtained by dividing the histogram of damaging shots by that of the total number of laser shots. The curve is the maximum likelihood estimate of the probability where a normal probability density distribution was assumed. The lower right hand graph is a probit plot of the same data. The probit is a coordinate transformation which linearizes the probability curve. The dashed lines represent 95% confidence limits based on Student's *t* distribution. The damage threshold corresponding to the 50% probability of damage occurs at 0.120 ± 0.002 V, which represents an irradiance of 4.0 J/cm^2 .

UNCLASSIFIED

10

N 4 SODA-LIME GLASS TUE 5 FEB 1980

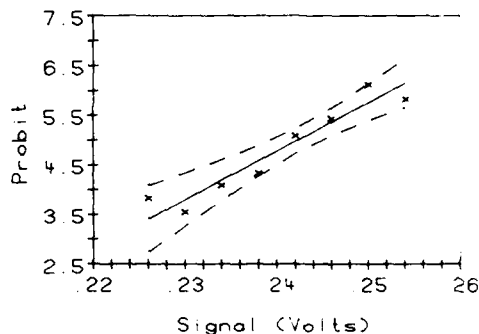
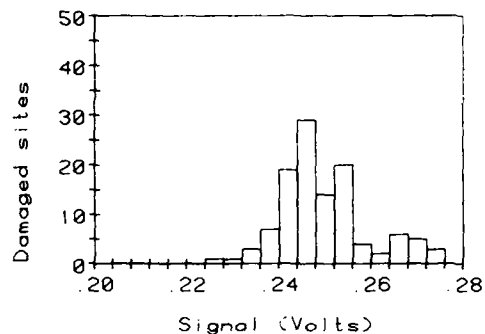
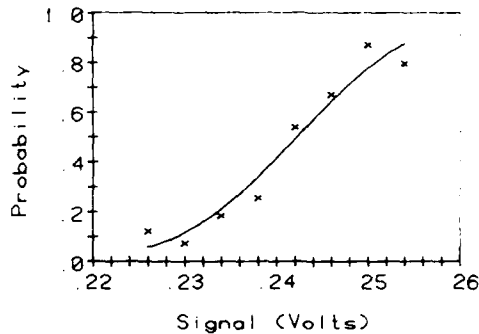
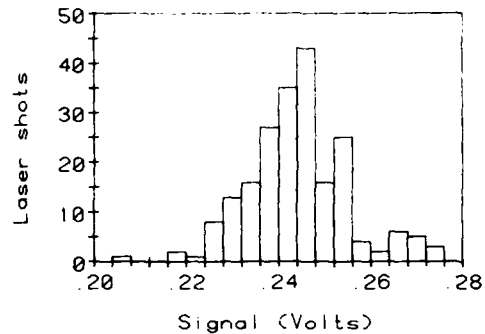


FIGURE 5 - Experimental results for the measurement of the damage threshold in soda-lime glass. An explanation of the graphs appears in the caption of Fig. 4. In soda-lime glass, damage is characterized by surface cracking. The threshold for a 50% probability of damage is 0.242 ± 0.003 V, corresponding to an irradiance level of 2.1 J/cm^2 .

UNCLASSIFIED

11

N 3 POLYCARBONATE PLASTIC NED 16 APR 1980

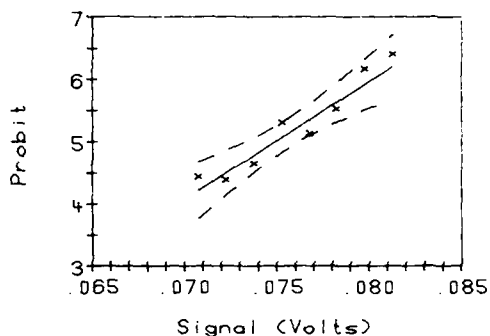
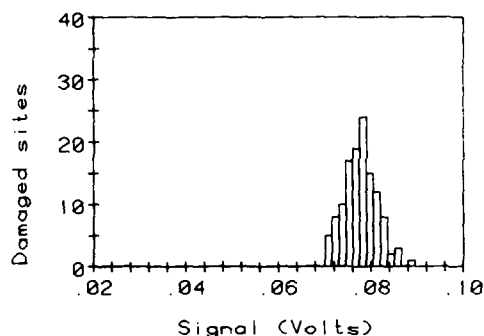
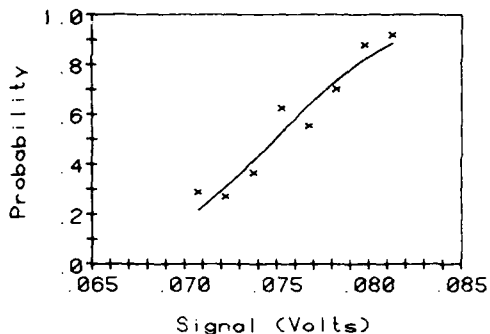
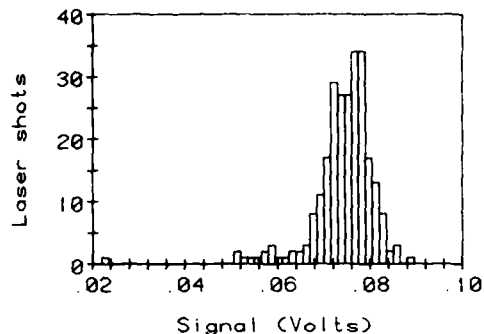


FIGURE 6 - Experimental results for the measurement of the damage threshold in polycarbonate plastic. An explanation of the graphs appears in the caption of Fig. 4. In polycarbonate, damage is characterized by surface melting. The threshold for a 50% probability of damage is 0.075 ± 0.001 V, corresponding to an irradiance level of 2.3 J/cm^2 .

UNCLASSIFIED

12

N 3 ACRYLIC PLASTIC WED 26 MAR 1980

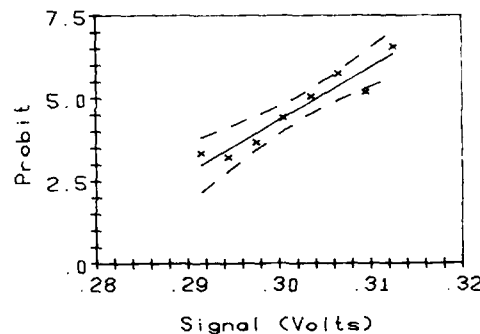
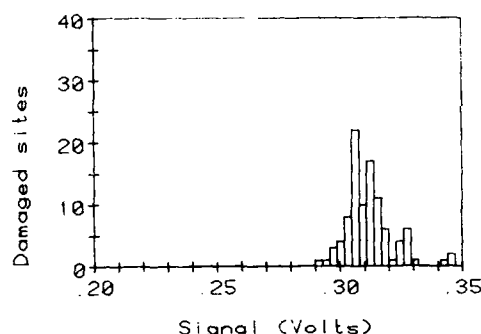
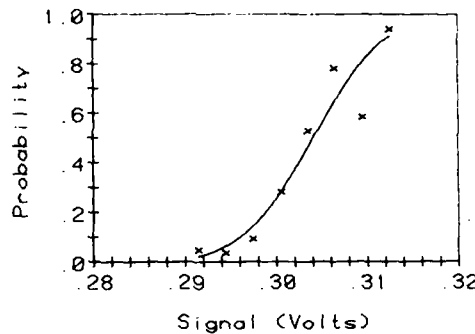
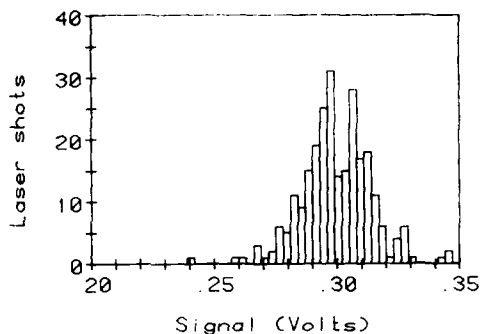


FIGURE 7 - Experimental results for the measurement of the damage threshold in acrylic (PMMA). An explanation of the graphs appears in the caption of Fig. 4. In PMMA, damage is characterized by surface melting. The threshold of a 50% probability of damage is 0.304 ± 0.003 V, corresponding to an irradiance level of 2.3 J/cm^2 .

UNCLASSIFIED

13

N 3 POLYSTYRENE PLASTIC VED 16 APR 1980

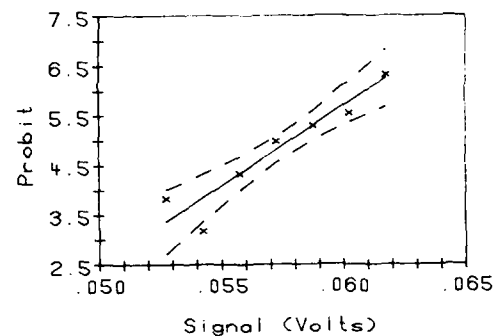
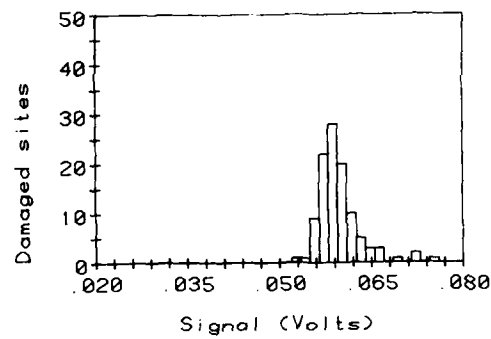
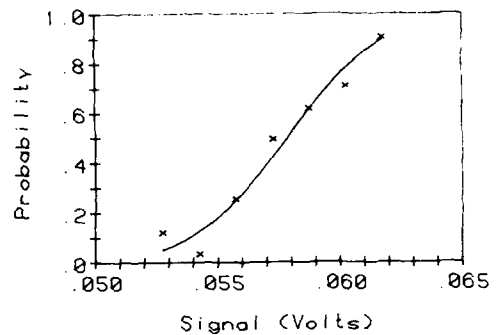
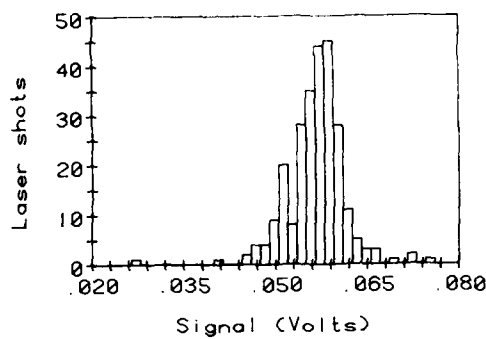


FIGURE 8 - Experimental results for the measurement of the damage threshold in polystyrene. An explanation of the graphs appears in the caption of Fig. 4. In polystyrene, damage is characterized by surface melting. The threshold for a 50% probability of damage is 0.0579 ± 0.0009 V, corresponding to an irradiance level of 1.7 J/cm^2 .

UNCLASSIFIED

14

3.0 STATISTICAL ANALYSIS OF DAMAGE MEASUREMENTS3.1 Sources of Statistics in Threshold Measurements

The five materials chosen for this series of experiments are strong absorbers of the 10.6- μm radiation from CO₂ lasers. Assuming that the absorption is homogeneous, one at first expects the damage due to the absorbed energy to be deterministic, i.e. free from statistics. A few measurements quickly showed that this is not strictly true as two, apparently similar, laser shots produced different results. The statistical nature of these results could arise from several causes such as fluctuations in the laser output, lack of material homogeneity, presence of localized dirt or polishing compounds, variations in the positioning of the sample, fluctuations of the laser beam profile, or the intrinsic way in which damage manifests itself after the laser energy is absorbed.

This experiment was designed to eliminate the effects of the variations in the laser output by accurately measuring the energy of each pulse. Lack of material homogeneity seems unlikely in our experiments since the sites were all on the same sample, and any small variations in the absorption are negligible compared to the 90% to 96% absorption (Ref. 12) for these materials. Although the samples were tested as received, their appearance ruled out any gross contamination by foreign substances. In any case, the absorption is not expected to be greatly affected by small amounts of imperceptible dirt. Variations in the positioning of the sample were reduced by ensuring that the scanning motion was parallel to the surface of the sample. A poor alignment of the scanner would have caused the damaged sites to collect in the same portion of the sample. Temporal variations in the laser pulses were not expected to affect results since those pulses were all nominally the same length, and any small variations

occurred over time periods much shorter than the diffusion time necessary for the irradiated areas to cool down. However, fluctuations in the beam profile and in the way damage occurs in glass do affect the results, as discussed in Section 4. Once all statistics due to extrinsic causes have been accounted for, those that remain must be attributed to intrinsic ones and they must be checked against their expected distribution.

3.2 Probit Analysis

The underlying assumption is that the probability for damage increases with the density of energy falling on the surface of the material. Furthermore, we assume that the threshold levels are normally distributed, with a variance related to the damage mechanism. If the energy density, or irradiation, is denoted by E , the probability distribution of damaged sites may be expressed by

$$dP = (2\pi\sigma^2)^{-1/2} \exp [-(E-\mu)^2/2\sigma^2] dE \quad [1]$$

where dP is the probability of damage occurring over the energy density range dE , μ is the mean of the distribution, and σ^2 is the variance.

The analysis used to estimate the parameters μ and σ^2 of eq. 1 is based upon the probit transformation of the experimental results (Ref. 13). The probit is the random variable which corresponds to the probability in a normal distribution, with mean 5 and variance 1. Symbolically, the probit, Y , of the probability, P , is defined by

$$P = (2\pi)^{-1/2} \int_{-\infty}^{Y-5} \exp[-u^2/2] du \quad [2]$$

Integration of eq. 1 gives the expected proportion of samples damaged up to an energy density E_0 as

$$P = (2\pi\sigma^2)^{-1/2} \int_{-\infty}^{E_0} \exp[-(E-\mu)^2/2\sigma^2] dE \quad [3]$$

Comparison of [2] and [3] shows that the probit of the expected damaged proportion is related to the energy density by the linear equation

$$Y = 5 + (E_0 - \mu)/\sigma \quad [4]$$

Traditionally, the probit method is to fit a best straight line to eq. 4, by adjusting μ and σ to obtain the maximum likelihood estimate for the experiment. That is, the two adjustable parameters of the distribution function are varied to obtain the probability distribution which corresponds to the results observed to be the most likely outcome of the experiment. In the past, the probit transformation was used to linearize the probability distribution and thus to facilitate this fitting. Although modern computers makes this no longer strictly necessary, expressing the results in terms of the probit is useful for comparison and interpretation. Our fitting procedure, which closely follows the method developed in Appendix II of Ref. 13, is performed in APL, as described in Appendix A. Once the maximum likelihood estimate of the probability distribution function has been obtained, it is easy to determine the energy density required for a given probability of damage. For a 50% probability of damage, the energy level required is equal to μ .

UNCLASSIFIED

17

Strictly, the probit refers only to the normal distribution. However, it is instructive to perform a similar analysis for a general distribution. In particular, the APL program we elaborated can also perform the analysis for a uniform distribution.

4.0 RESULTS AND DISCUSSION

With an APL program, we scaled and sorted the raw data into two histograms, one of the total number of laser shots, the other for those shots causing damage as a function of joulemeter voltage. Following the probit analysis, the data was displayed graphically, as shown in Figs. 4 to 8, for fused silica, soda-lime glass, polycarbonate, acrylic and polystyrene plastics respectively. In each of those figures the upper left graph is the histogram of all laser shots plotted as a function of the joulemeter signal voltage proportional to the energy density of the beam at the target. The lower left graph is the histogram of those shots which damaged the surface. The upper right graph shows the probability of causing damage as a function of the joulemeter voltage. The crosses represent the relative frequencies of damage obtained by dividing the histogram of damaging shots by that of the total number of laser shots. The curve is the maximum likelihood estimate of a normal probability density distribution. The lower right graph is a probit plot of the same data. The dashed lines represent the 95% confidence limits based on Student's t distribution.

We define the damage thresholds as the energy density levels at which the probability of damage is 50%. Table I gives the values obtained for the thresholds, and the standard deviation of the probability distribution function.

UNCLASSIFIED

18

TABLE I

Damage Threshold for Various Optical Materials

MATERIAL	THRESHOLD (μ) (J/cm 2)	STANDARD DEVIATION (σ) (J/cm 2)	COEFFICIENT OF VARIATION (σ/μ)
Fused silica	4.0 (.03)*	0.31 (0.06)	0.076 (.016)
Soda-lime glass	2.1 (.01)	0.089 (0.01)	0.042 (.007)
Polycarbonate plastic	2.3 (.02)	0.16 (0.03)	0.071 (.013)
Acrylic plastic	2.3 (.01)	0.047 (0.01)	0.021 (.005)
Polystyrene plastic	1.7 (.01)	0.091 (0.01)	0.054 (.008)

* Numbers in parentheses are the standard deviations of the estimates for the parameters of the probability distribution function.

U 3 ACRYLIC PLASTIC WED 26 MAR 1980

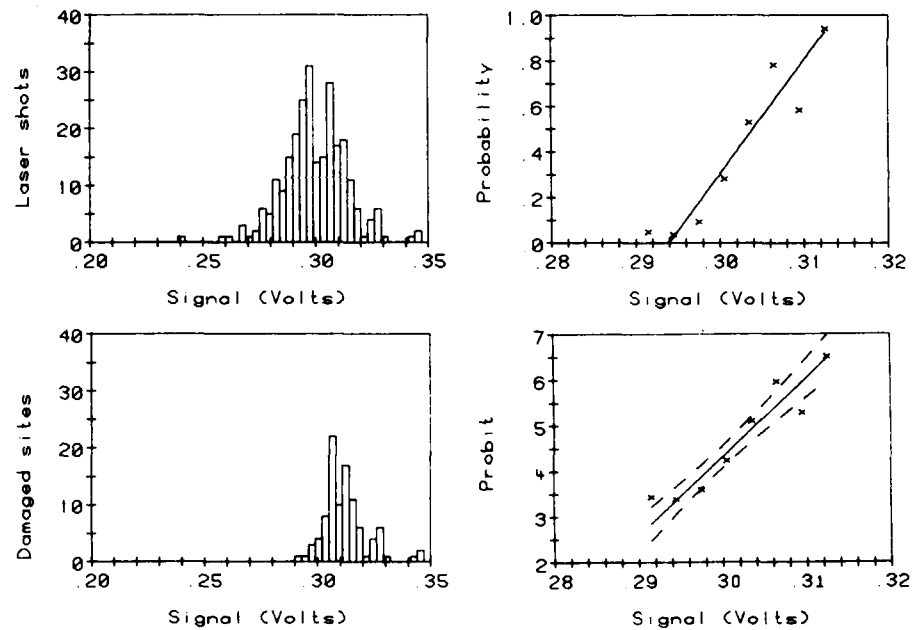


FIGURE 9 - Analysis of the experimental results for acrylic plastic assuming a uniform density for the probability density function. A full explanation of the graphs appears with Fig. 4. The estimated energy density for a 50% probability of damage occurs at 0.304 ± 0.002 V, corresponding to an energy density of 2.3 J/cm^2 . This result differs insignificantly from that obtained using a normal distribution function.

Figure 9 illustrates the results of the soda-lime glass analysis when a uniform probability distribution is used. The results for σ and μ only slightly differ from those of the normal distribution in Fig. 5. There is no significant difference between the two distributions for representing the experimental data. This holds for the other materials as well.

The coefficient of variation, (σ/μ), is an estimate of the relative dispersion in the threshold data. As shown in Table I, this coefficient is small for all materials tested. The finite binwidths used in calculating the estimates had no significant effect since Sheppard's correction was negligible and recalculation of the estimates of σ showed no changes, even when bins several times larger were used.

The experiments on the fused silica, polycarbonate, and polystyrene samples yielded the largest coefficients of variation. Since it meant looking for surface distortions due to melting, detecting damage in these three materials was difficult. In fact, their melting points are ill-defined and the recorded deflection and heat resistance temperatures factors for plastics vary greatly (Ref. 14). Some of the variations in the reported temperatures can be attributed to differences between manufacturing processes or batches. On the other hand, silica is a true glass; it does not 'melt', but because of a decreasing viscosity, it becomes softer with increasing temperature.

However, the cracks in the glass and the white spots in the PMMA samples were readily seen and gave a clear indication of the damage occurrence. Therefore, the dispersions observed in the fused silica, polycarbonate and polystyrene seem largely due to the damage detecting method. The observations in PMMA and glass likely reflect other causes.

UNCLASSIFIED

20

The damage in PMMA consisted of many voids, $\sim 10 \mu\text{m}$ in size, lying in the surface (Fig. 10). There is little evidence of ejected debris. This, and the strong solvent-like odor exhaled during the experiments suggest that damage occurred when the plastic decomposed into volatile substances which evaporated under the laser heating. The narrow dispersion in the measured damage thresholds indicates that this decomposition occurs at a well defined temperature.

On the other hand, the glass failed by thermal fracture, as shown in Fig. 11. It is possibly because the surface first undergoes compressive stress, due to thermal expansion when heated by the laser beam, then partially relaxes as a viscous flow relieves some of the stress, at high temperatures, when the viscosity of glass drops dramatically and finally contracts on cooling to produce a tensile stress sufficient to cause failure by fracture. Temperature increases of $\sim 750^\circ\text{C}$ will cause that type of failure in soda-lime glass. To induce failure in fused silica, the temperature changes must exceed 2000°C . Such temperatures being well above the point where silica flows easily, damage in this material would first appear as surface distortion due to melting.

The surface of glass can be abraded during handling. The flaws thus created control the fracture by concentrating stresses and causing failure at levels much lower than the theoretically predicted loads calculated from the forces between the atoms of the glass. Therefore, the distribution of these flaws is expected to be reflected in the distribution of failure thresholds for laser damaging of glass. Fisher and Hollomon (Ref. 15) investigated the theoretical distribution of stress failure in glass for simple and hydrostatic tensions as well as unidirectional tension with equal bidirectional compression. They assumed an exponential distribution of flaw sizes and used the Griffith

UNCLASSIFIED

21



FIGURE 10 - Scanning electron micrograph of a sample of PMMA damaged by a 34- μ s CO₂ laser pulse at 8.3 J/cm². Damage consists of many voids caused by the evaporation of the monomer produced when the material is depolymerized by heating.

UNCLASSIFIED

22



FIGURE 11 - Micrograph of the surface of a sample of soda-lime glass damaged by a 34- μ s CO₂ laser pulse at 2.8 J/cm². Fracture lines due to thermal stress are evident. An above threshold irradiance was used to produce a large number of fractures. Under the assumption that the fractures occur at micro cracks in the surface, a minimum density of 15 000 cracks per cm² must have been present to produce the observed results.

UNCLASSIFIED

23

model in which the failure strength of a defect is inversely proportional to the square root of its length. The theory may be extended to include the stress induced by laser heating of the surface. In this case, there is tensile stress in two directions parallel to the surface but no stress perpendicular to it. Qualitatively, the results are similar to those obtained in Ref. 15 for the other stress fields. Figure 12 illustrates the frequency distributions for fracture stresses in laser-heated glass samples as a function of the number of crack flaws. There is a marked decrease in the mode and mean of the distribution as the number of cracks increases. More explicitly, the most probable failure-causing stress (the stress for which there is a 50% probability of failure) drops as more defects are included within the laser heated region. The dispersion of the fracture values also decreases as the number of cracks increases. As Fig. 11 shows, the distance between fractures is 60 to 80 μm , indicating a crack density of at least 15 000 to 30 000 per cm^2 . For the 12-x12-mm spot size of these experiments, this corresponds to 20 000 to 36 000 defects. The coefficient of variation for a distribution with this number of cracks ranges from 0.061 to 0.065. This is approximately 50% higher than the coefficient of variation we observed during our experiments and it requires a crack density of $\sim 3 \times 10^6$ per cm^2 . Since the distribution of flaws is not the only factor accounting for the observed variation, it appears that even more defects are required to explain the results with this simple model.

From measurements of the fracture strength of glass, Fisher and Hollomon (Ref. 15) estimated a flaw density of $\sim 1\ 000$ per cm^2 of surface area. The dispersion observed in the threshold experiment thus requires a density of flaws much greater than expected, even when the 15% to 20% standard deviation of the coefficient of variations is considered. During the glass heating phase, the compressional

UNCLASSIFIED

24

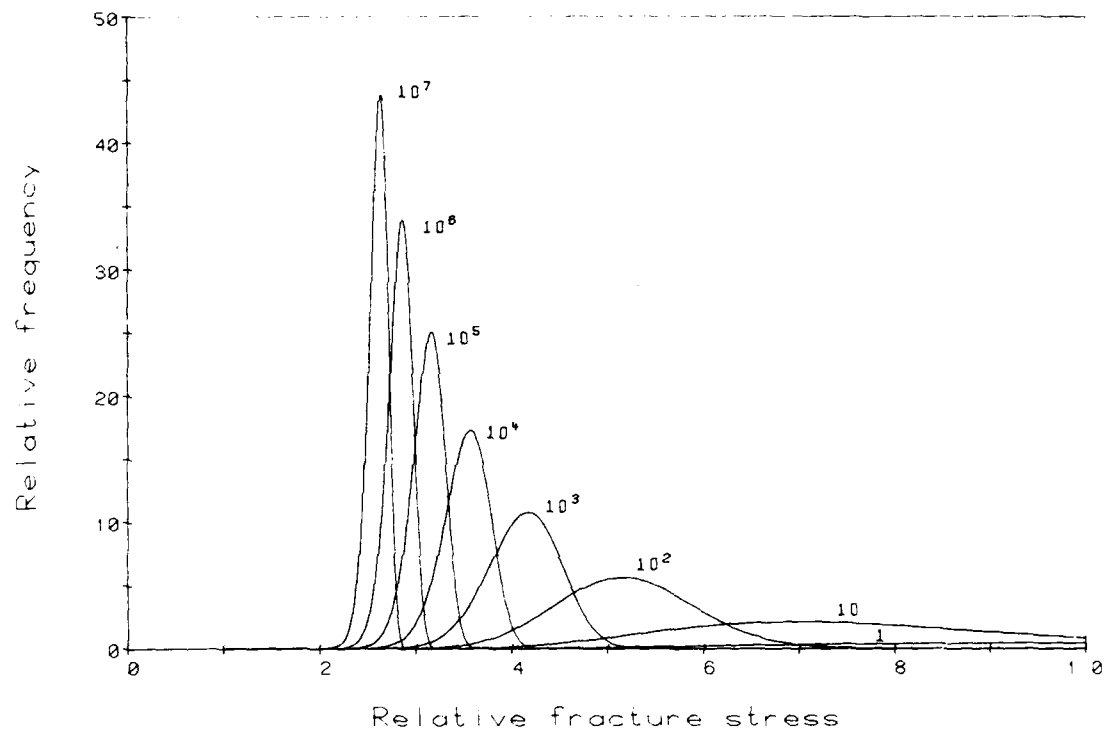


FIGURE 12 - Frequency distributions of fracture stresses for glass samples containing 1 to 10^7 cracks. The normalized curves represent the probability distribution functions for failure as a function of uniform tensile stress parallel to the surface of the sample. As the number of cracks present increases the most probable and mean failure stresses decrease and the dispersion also diminishes.

UNCLASSIFIED

25

stresses produce shear stresses in any cross section that is not parallel to the surface. These stresses may exceed the dynamic shear strength of the glass and produce many small cracks or enlarge those already present, so that the distribution of flaws is significantly altered by the time the tensile stress develops. It is also possible that our glass samples initially had more relatively large crack flaws since they were not protected against abrasions during handling.

Determining the irradiance level from the total beam energy and the beam profile is the main source of error. The absolute calibration of the joulemeter is known to within $\sim 5\%$ and variations in the height of the beam profile are $\sim 10\%$. Uncertainties in the latter could be reduced considerably by space filtering the beam and by accurately measuring its profile with a pyroelectric vidicon camera. These refinements will be incorporated for future measurements. We estimate that the overall accuracy of the threshold levels obtained with the current arrangement is 15% - 20%, when the accuracy of the measuring and recording instruments and the calibration of the energy monitoring technique are included.

5.0 CONCLUSION

We described an apparatus and a method for measuring the magnitude and the statistical distribution of the laser irradiations required to damage various glass and plastic surfaces. We determined threshold levels for a 50% probability of damage by $\sim 34 \mu s$ TEA-CO₂ laser pulses for fused silica, common window glass, clear acrylic, polycarbonate, and polystyrene sheet plastics. Significant statistics were observed for all materials, except for the acrylic plastic whose dispersion was at the limit of the experimental technique. The mechanism of laser induced damage varies for the different materials. The fused silica, polycarbonate, and polystyrene specimens failed by

UNCLASSIFIED

26

surface melting, and have relatively large dispersions, showing that their melting points are not well defined. The acrylic plastic decomposed at a well defined level and soda-lime glass failed by thermal fracture over a narrow but finite range. The number of surface flaws required to explain the narrow dispersion of threshold irradiation levels measured in soda-lime glass is larger than expected from glass strength measurements.

6.0 ACKNOWLEDGEMENTS

We thank Dr. M. Gravel for many helpful discussions, Messrs. C. Trepanier and G. Boily who performed the damage experiments, and Mr. W. Pille who designed the interface between the data acquisition system and DREV's main computer.

UNCLASSIFIED

27

7.0 REFERENCES

1. Bass, M. and Barrett, H.H., "The Probability and Dynamics of Damaging Optical Materials with Lasers", Damage in Laser Materials: 1971, edited by Glass, A.J. and Guenther, A.H., NBS Special Publication 356, U.S. Govt. Printing Office, Washington, p. 76, 1971.
2. DeShazer, L.G., Newman, B.E. and Leung, K.M., "The Role of Coating Defects in Laser-induced Damage to Thin Films," Laser Induced Damage in Optical Materials: 1973, edited by Glass, A.J. and Guenther, A.H., NBS Special Publication 387, U.S. Govt. Printing Office, Washington, p. 114, 1973.
3. DeShazer, L.G., Newman, B.E. and Leung, K.M., "Role of Coating Defects in Laser-induced Damage to Dielectric Thin Films", Appl. Phys. Lett., Vol. 23, pp. 607-609, 1973.
4. Bliss, E.S., Milam, D., Bradbury, R.A., "Dielectric Mirror Damage by Laser Radiation over a Range of Pulse Durations and Beam Radii", Appl. Opt., Vol. 12, pp. 677-689, 1973.
5. Milam, D., Bradbury, R.A., Picard, R.H. and Bass, M., "Laser-Damage-Mechanism Identification by the Measurement of Survival Times", Laser Induced Damage in Optical Materials: 1974, edited by Glass, A.J. and Guenther, A.H., NBS Special Publication 414, U.S. Govt. Printing Office, Washington, p. 169, 1974.
6. Hacker, M.P. and Halverson, W., "Method for Accurate Determination of Threshold Pulse Energies for Laser-induced Gas Breakdown", Rev. Sci. Instrum., Vol. 47, pp. 634-636, 1976.
7. Laflamme, A.K., "Double Discharge Excitation for Atmospheric Pressure CO₂ Lasers", Rev. Sci. Instrum., Vol. 41, pp. 1578-1581, 1970.
8. Beaulieu, A.J., "Transversely Excited Atmospheric Pressure CO₂ Lasers", Appl. Phys. Letters, Vol. 16, pp. 504-505, 1970.
9. Heenan, R.S. and Nilson, J.A., "Final Report Pulse Length Control of TEA-CO₂ Lasers", Lumonics Technical Report LTM 2-76, April 14, 1976.

UNCLASSIFIED

28

10. Kembry, K. and MacPherson, R.W., "CO₂ Laser Induced Breakdown and Damage to Surfaces of Laser Optical Materials", DREV Technical Note 2013/72, July 1972, UNCLASSIFIED
11. MacPherson, R.W., "Variable Attenuator for TEA-CO₂ Lasers", Rev. Sci. Instrum., Vol. 45, pp. 316-317, 1974.
12. Delisle, Prof. C. and Girard, A., "Etude de la pénétration des rayonnements infrarouges dans les substances diélectriques opaques", Laboratoire de recherches en optique et laser, Université Laval, Québec, 1979.
13. Finney, D.J., "Probit Analysis", Cambridge University Press, Cambridge, 1952.
14. "1973-1974 Modern Plastics Encyclopedia", Vol. 50, No 10A, McGraw-Hill Inc., New York, Oct. 1973.
15. Fisher J.C. and Hollomon J.H., "A Statistical Theory of Fracture", Metals Technology, Vol. 14, Technical Publication No. 2218, 1947.
16. Conklin, T. and Stupp, E.H., "Applications of the Pyroelectric Vidicon", Optical Engineering, Vol. 15, No. 6, pp. 510-515, 1976.
17. Griffith, A.A., International Congress for Appl. Mech., Delft, p. 61, 1924.

UNCLASSIFIED

29

APPENDIX AMaximum Likelihood Estimation by the Probit Method

Under the assumption that eq. 1 represents the probability distribution function (p.d.f.) of the damage producing energy densities, the probability of damage occurring at an energy density, E, is given by eq. 3 for the normal distribution or by

$$P = \begin{cases} 0 & \text{if } Y < 5 - \sqrt{3} \\ (Y-5+\sqrt{3})/2\sqrt{3} & \text{if } |Y-5| < \sqrt{3} \\ 1 & \text{if } Y > 5 + \sqrt{3} \end{cases}$$

for the uniform distribution.

In a batch of n samples, irradiated at a level E, independently of one another, the probability of r being damaged is

$$P(r) = [n! / r!(n-r)!] P^r [1 - P]^{n-r} \quad [A1]$$

Consequently, the probability of a particular experiment in which the number of damaged sites is counted for a variety of k irradiation levels to occur is

$$P = \prod_{i=1}^k [n_i! / r_i!(n_i - r_i)!] P_i^{r_i} [1 - P_i]^{n_i - r_i} \quad [A2]$$

The maximum likelihood method consists in determining the values of the parameters of P which maximize P.

The regression equation used in the probit method was given in eq. 4 as

$$Y = 5 + (x - \mu)/\sigma \quad \text{or}$$

$$Y = \alpha + \beta x \quad [A3]$$

where $\alpha = 5 - \mu/\sigma$ and $\beta = 1/\sigma$.

The solution to this equation is detailed in Appendix II of Ref. 13 and is found by solving the following two equations for α and β .

$$\begin{aligned} \alpha \sum_{i=1}^k n_i w_i + b \sum_{i=1}^k n_i w_i x_i &= \sum_{i=1}^k n_i w_i y_i \\ \alpha \sum_{i=1}^k n_i w_i x_i + b \sum_{i=1}^k n_i w_i x_i^2 &= \sum_{i=1}^k n_i w_i x_i y_i \end{aligned} \quad [A4]$$

where α is the maximum likelihood estimate for α ,

b is the maximum likelihood estimate for β ,

$$y_i = y_i + (p_i - P_i)/Z_i,$$

$$w_i = Z_i^2/P_i(1 - P_i),$$

n_i = number of sample sites tested at energy density level E_i ,

x_i = Joulemeter signal volts corresponding to E_i ,

p_i = r_i/n_i where r_i is the number of damaged sites at level E_i ,

y_i = the probit corresponding to x_i ,

and $Z_i = (2\pi)^{-1/2} \exp[-(Y_i - 5)^2/2]$ for the normal distribution,

or $Z_i = \begin{cases} 1/2\sqrt{3} & \text{if } |Y_i - 5| < \sqrt{3} \\ 0 & \text{if } |Y_i - 5| > \sqrt{3} \end{cases}$ for the uniform distribution.

UNCLASSIFIED

31

Since the summations in eq. A4 are functions of Y and hence also of α and b , the solution to eq. A4 must be found iteratively. The procedure is to start with reasonable guesses α_1 , b_1 to α and β , calculate Y from eq. A3, perform the indicated sums, and solve eq. A4 for new estimates α_2 and b_2 . The process is repeated with $Y = \alpha_2 + b_2x$ and continued until a consistent solution is obtained within the desired accuracy. This procedure is performed with the APL program PFIT in which the criteria used to test for convergence to a solution is $[\|\alpha_{j+1} - \alpha_j\|/\alpha_j + \|b_{j+1} - b_j\|/b_j] < 10^{-6}$, where j is the iteration number. Once α and b are found, the parameters of the p.d.f. are determined from:

$$m = (5 - \alpha)/b$$

[A5]

$$\hat{\sigma} = 1/b$$

The variances of the parameters appearing in the computer program are calculated as follows.

$$V(\bar{y}) = 1 / \sum_{i=1}^k n_i w_i$$

$$V(\alpha) = \bar{x}^2/S_{xx}$$

$$V(m) = [V(\bar{y}) + (m - \bar{X})^2/S_{xx}] / b^2$$

$$V(\hat{\sigma}) = V(b)/b^4$$

$$V(\hat{\sigma}/m) = [V(\bar{y}) + (\bar{X})^2/S_{xx}] / b^4 m^4$$

The fiducial limits to Y are calculated from $Y \pm t \sqrt{V(Y)}$ where t is the Student's t deviate for the 95% level of probability used. The fiducial limits for x corresponding to a given probit Y are given by

UNCLASSIFIED

32

$$x + g(x - \bar{x})/(1 - g) \pm t[(1 - g)V(\bar{y}) + (x - \bar{x})^2/S_{xx}]^{1/2}/b(1 - g)$$

where $g = t^2/b^2S_{xx}$.

Table A1 lists and describes the important APL variables found in the program. The listing appears in Table A2. Table A3 is a sample program output for the fused silica case of Fig. 4.

UNCLASSIFIED

33

TABLE A1

Variables used in PFIT program

<u>APL Name</u>	<u>Variable Name</u>	<u>Description</u>
<i>PDF</i>	-	p.d.f. identifier flag ' <i>N</i> ' for Normal, ' <i>U</i> ' for uniform
<i>RNX</i>	-	matrix of $\{r_i, n_i, x_i\}$
<i>IFG</i>	-	convergence flag = 0 for no convergence = 1 for convergence
<i>LL</i>	-	mask for empty bins or bins with no deaths or no survivors (i.e. no sites damaged or all sites damaged at a particular E_i)
<i>P</i>	P_i	relative frequency r_i/n_i for signal voltage x_i
<i>XX</i>	x_i	signal voltage
<i>S</i>	σ	maximum likelihood estimate of σ , the standard deviation of the p.d.f.
<i>M</i>	m	maximum likelihood estimate of μ , the mean of the p.d.f.
<i>A</i>	a_i, b_i	value of fitted parameters before iteration <i>i</i>
<i>NA</i>	a_{i+1}, b_{i+1}	value of fitted parameters after iteration <i>i</i>
<i>Y</i>	y	estimated probit
<i>P</i>	p	estimated probability
<i>Z</i>	z	p.d.f. $Z_i = (2\pi)^{-1/2} \exp. [-(y_i - 5)^2/2]$ for the normal distribution or
<i>W</i>	$\sqrt{n_i w_i}$	$Z_i \begin{cases} = 1/2\sqrt{3} & \text{if } y_i - 5 < \sqrt{3} \\ = 0 & \text{otherwise for the uniform distribution} \end{cases}$
<i>YY</i>	-	weight factor where $w_i = Z_i^2/P_i(1 - P_i)$ matrix of sums in eq. A4 =
		$\begin{bmatrix} \sum_{i=1}^k n_i w_i & \sum_{i=1}^k n_i w_i x_i & \sum_{i=1}^k n_i w_i y_i \\ \sum_{i=1}^k n_i w_i x_i & \sum_{i=1}^k n_i w_i x_i^2 & \sum_{i=1}^k n_i w_i x_i y_i \end{bmatrix}$

UNCLASSIFIED

34

<u>APL Name</u>	<u>Variable Name</u>	<u>Description</u>
XB	\bar{x}	$\frac{\sum_{i=1}^k n_i w_i x_i}{\sum_{i=1}^k n_i w_i}$
YB	\bar{y}	$\frac{\sum_{i=1}^k n_i w_i y_i}{\sum_{i=1}^k n_i w_i}$
Sxx	S_{xx}	$\sum_{i=1}^k n_i w_i (x_i - \bar{x})^2$
SXY	S_{xy}	$\sum_{i=1}^k n_i w_i (x_i - \bar{x})(y_i - \bar{y})$
SYy	S_{yy}	$\sum_{i=1}^k n_i w_i (y_i - \bar{y})^2$
$CHID$	-	$n_i w_i (p_i - P_i)^2 / Z_i^2$ = contribution of i^{th} point to chi square parameter.
CHI	χ^2	chi square parameter = $\sum_{i=1}^k n_i w_i (p_i - P_i)^2 / Z_i^2$
HET	χ^2/v	heterogeneity factor
NU	v	number of degrees of freedom; $v=k-2$
$HETF$	-	max.(1, HET) heterogeneity factor multiplying variances
VM	$V(m)$	variance of m
VIY	$V(Y)$	variance of Y

UNCLASSIFIED

35

<u>APL name</u>	<u>Variable Name</u>	<u>Description</u>
<i>VS</i>	$V(\sigma)$	variance of $\sigma = \sigma^4 V(b)$
<i>VA</i>	$V(\alpha)$	variance of $\alpha = 1/\sum_{i=1}^k n_i w_i$
<i>VB</i>	$V(b)$	variance of $b = 1/Sxx$
<i>T</i>	t	parameter in Student's t distribution (includes heterogeneity factor) for calculating confidence limits
<i>G</i>	g	$g = t^2/b^2 Sxx$
<i>MD</i>	-	$[t/b(1-g)][(1-g)/\sum w_i + (\bar{x}-\bar{\bar{x}})^2/Sxx]$ terms used in fiducial limits of m
<i>MB</i>	-	$x + g(x-\bar{x})/(1-g)$

UNCLASSIFIED

36

TABLE A2

Program Listings

```

VPEP PPIP RYX;LL;UL;S;W;X;YY;W;D;Y;IFG;GET;XB;YB;C4ID;V
S4;V4;V5;V64;G
[1]  $\alpha \bar{X} = R, [1] V, [.5] X$ 
[2]  $\alpha D = 'V' \text{ FOR NORMAL DISTRIBUTION, 'U' FOR UNIFORM DISTR$ 
 $\text{IBUTION.}'$ 
[3]  $I\#G \leftarrow 0$ 
[4]  $\text{START WITH AT LEAST ONE DEATH, END WITH AT LEAST ONE}$ 
 $\text{SURVIVOR}$ 
[5]  $\text{READ IN EMPTY BINS}$ 
[6]  $LL \leftarrow 0, RYX[1];$ 
[7]  $LL + LL * 1 \# P \leftarrow ; \# - 1 \# RYX$ 
[8]  $P \leftarrow LL / ?$ 
[9]  $\bar{X} \leftarrow LL / RYX[3];$ 
[10]  $A$ 
[11]  $\text{ESTIMATE STARTING PARAMETERS}$ 
[12]  $A$ 
[13]  $S \leftarrow .5 * [1] \# RYX[1, P \# X]$ 
[14]  $S0 : W \leftarrow .5 * + / RYX[1, P \# X]$ 
[15]  $IA \leftarrow (S - 4 * S), + S$ 
[16]  $S1 : A \leftarrow IA$ 
[17]  $Y \leftarrow 1[1] + 4[2] \# XX$ 
[18]  $S0 : \rightarrow (PD = 'VU') / SW, SJ$ 
[19]  $I * 'PD'  $34$ ABILITY MUST BE U OR V. RETYPE.'$ 
[20]  $PD \leftarrow I$ 
[21]  $\rightarrow S0$ 
[22]  $S4 : P \leftarrow PR03N(Y-5)$ 
[23]  $Z \leftarrow (P \# 1) * (P \# 0) * ((P \# 0) * .5) * * -.5 * (Y-5) * 2$ 
[24]  $\rightarrow S2$ 
[25]  $SJ : P \leftarrow (Y-5 + 3 * .5) / 2 * 3 * .5$ 
[26]  $\# IF G \neq 1$ 
[27]  $P \leftarrow P * P > 0$ 
[28]  $P \leftarrow (P * P < 1) + P > 1$ 
[29]  $Z \leftarrow (.5 * 3 * .5) * (3 * .5) > | Y-5$ 
[30]  $S2 : \rightarrow ((LL / RYX[2, 1]) * Z * Z * ((P \# 0) * P) * ((P \# 1) / 1 - P)) * .5$ 
[31]  $\alpha Z = 0 SET TO Z = 1 TO VOID + 0. WEIGHT, W, HAS Z FACTOR$ 
 $\text{TO TAKE SUMMING CORRECT LATER.}$ 
[32]  $YY \leftarrow Y + (Z - P) / 2 + Z = 0$ 
[33]  $X \leftarrow X + .5 * \bar{X} (X \leftarrow W, [.5] W * XX), [1] + * YY$ 
[34]  $\rightarrow (I\#G = 1) / S4$ 
[35]  $.4 \leftarrow , X[3] \# X[1, 2]$ 
[36]  $\rightarrow (TOL \leftarrow + / | - 1 + VA \# A) / S1$ 
[37]  $I\#G \leftarrow 1$ 
[38]  $\rightarrow S1$ 
[39]  $A$ 
[40]  $\text{READ PPIP RESULTS}$ 

```

UNCLASSIFIED

37

[41] A
[42] S4: A←(S-N1[1])÷N4[2]
[43] S←N1[2]
[44] X3←X[1;2]÷X[1;1]
[45] Y3←X[1;3]÷X[1;1]
[46] SXA←X[2;2]-X5×X[2;1]
[47] SYX←X[2;3]-X6×X[1;3]
[48] SYY←(+/SYY×SYY+YY×N)-Y3×X[1;3]
[49] CYI←/CYID←CYI×CHI←✓×(P-P)÷J
[50] YH2←CYI÷IJ←-2+pXX
[51] YET←1[YET]
[52] V4←S×S×(:X[1;1])+((N-XB)*2)÷SXX
[53] VY←VTF×(:X[1;1])+((XX-XB)*2)÷SXX
[54] VS←(S*4)÷SXX
[55] VS4←((:X[1;1])+XB×XB÷SXX)×(S÷4)*4
[56] VA←A[2;2]÷A[1;1]
[57] VB←÷SXX
[58] P←(VTF*.5)×((NJ≥4)×1.96+2.392÷NJ-1.032)+(3.18×NJ=5)+(4.3×NJ=2)+12.71×NJ=1
[59] G←P×P×S×S÷SXX
[60] ND←V4-G×S×S÷A[1;1]
[61] MB←(A-G×XB)÷1-G
[62] 'MTHRESHOLD(.50) = N,F10.5,T (N,F6.5,T)T'a(V;(VTF×V4)*.5)
→(ND≤0)/71
[64] ND←(P÷1-G)×4D*.5
[65] →(G<1)/H2
[66] →(A<XB)/H3
[67] 'LOWER FIDUCIAL LIMIT (.95): N > N,F8.5'αMB+4D
[68] →N4
[69] N1:'YO FIDUCIAL LIMITS AT EXIST .95 LEVEL'
[70] →N4
[71] N2:'N.95 FIDUCIAL LIMITS : N,F7.5,T+/-N,F6.5,T (N,F7.5,
, T < A < N,F7.5,T)T'a(MB;ND;45-4D;MB+4D)
[72] →N4
[73] N3:'UPPER LIMIT (.95): N < N,F8.5'αMB-4D
[74] N4:'COVARIANCE OF THE MEAN = N,F20.15'αVA×HETF
[75] 'STANDARD DEVIATION = N,F10.5,T (N,F8.6,T)T'a(S;(VTF
×VS)*.5)
[76] 'RATIO S/A = N,F6.4,T (N,F6.4,T)T'a(S÷A;(VTF×VS)*)*.5
)
[77] 'ONE SIG(A,I2,B) = N,F6.3'a(NJ;CHI)
[78] 'TEST FOR HOMOGENEITY FACTOR (APPLIED IFF >1) = N,F5.3'aVTF
[79] 'PARAMETERS'
[80] 'A = N,F10.5,T B = N,F10.6'α1 2p/4

UNCLASSIFIED

38

```

[81] 'VA = 1,F10.6,0      VB = 1,F11.6' a1 2p(TET←NETE★.S)×V
    A,VB
[82] 'V<X> = 1,F10.6,0      <Y> = 1,F10.6'a(Xb;YB)
[83] 'V SW = 1,F10.6,0      1/SW = 1,F12.10'a(X[1;1];X[1;1])
[84] 'V SX = 1,F10.6,0      SY = 1,F10.6'a1 2pX[1;2 3]
[85] 'V SX2 = 1,F10.6,0      SX.Y = 1,F10.6'a1 2pX[2;2 3]
[86] 'V SXA = 1,F10.6,0;    SX.Y = 1,F10.6,0;    SYY = 1,F10.6'a(S
    XX;SX;SY;SYY)
[87] '
[88] '
[89] ' X      N      R      P      PROBIT      Y      NW      YY      N
    WX      WY      ΔCHI
[90] '
[91] 'F5.3,2I4,F5.2,F7.2,2F8.3,F6.2,2F9.3,F6.3'a(XX;LL/RWX[2];
    2];LL/RWX[1];P;PDF PROBIT P;Y;W×W;YY;W×W×XX;W×W×Y;CH
    ID)
    V

```

VPROBN[0]v

VQ←PROBN X;B;T

```

[1] #CALCULATES NORMAL DISTRIBUTION PROBABILITY FUNCTION
[2] B←((pX),5)p.31938153 -.355563782 1.781477937 -1.821255
    978 1.330274429
[3] Q←(Q×(X<0))+((X≥0)×1-Q+((02)×-.5)×(+/B×(+1+.2316419×|X)
    ×.×15)××-X×X÷2
    V

```

VPROBIT[0]v

VZ←PDF PROBIT X

```

[1] →(PDF='704')/S1,S2,S3
[2] S1:Z←PROBIT4 X
[3] →0
[4] S2:Z←PROBITU X
[5] →0
[6] S3:Z←PROBITW X
[7] →0
    V

```

VPROBITW[0]v

VY←PROBITW P;T;Z

```

[1] d←|(P>.5)-P
[2] t←(-2×d)×.5
[3] Y←T-(2.5155177×.802853+T×.010328)+(1+7×1.432788+T×.13
    92+.001308×T)
[4] Y←5+Y×(-1)×P<.5
    V

```

UNCLASSIFIED

39

$$[1] \quad VY \leftarrow PROBITU P$$

$$Y \leftarrow (P \times 2 \times 3 * .5) + 5 - 3 * .5$$

$$V$$

TABLE A3Sample Output

FUSED SILICA WVN 28 APRIL 1980

THRESHOLD(.50) = .11978 (.00039)
 .95 FIDUCIAL LIMITS : .11975 +/- .00229 (.11745 < Y < .12204)
 VARIANCE OF THE MEAN = .0000799097588
 STANDARD DEVIATION = .00917 (.001912)
 RATIO S/V = .0766 (.0160)
 CHI SQ (9) = 2.489
 HETEROGENEITY FACTOR (APPLIED IFF >1) = .277
 PARAMETERS
 A' = -8.057728 B = 109.014407
 VA = .014392 VB = 516.321202
 $\langle X \rangle$ = .119890 $\langle Y \rangle$ = 5.012060
 SW = 105.371089 1/SW = .0094902692
 SX = 12.632999 SY = 528.126243
 SX2 = 1.516512 SX.Y = 63.528439
 SXX = .001937; SXY = .211137; SYY = 25.506211

X	N	R	P	EXPT'L		Y	NW	YY	NWX	NWY	ACHI
				PROBIT							
.111	7	1	.14	3.93	4.070	3.232	3.94	.360	13.157	.054	
.114	25	7	.28	4.42	4.397	13.929	4.42	1.591	61.250	.005	
.116	19	7	.07	4.66	4.561	11.273	4.67	1.305	51.411	.125	
.117	16	5	.71	4.51	4.724	9.908	4.52	1.162	45.805	.418	
.119	16	8	.50	5.00	4.898	10.139	5.00	1.204	49.558	.129	
.120	21	10	.48	4.94	5.051	13.356	4.94	1.605	67.466	.165	
.122	22	13	.59	5.23	5.215	13.773	5.23	1.677	71.821	.003	
.123	10	7	.70	5.52	5.378	5.042	5.52	.745	32.498	.121	
.125	20	15	.75	5.67	5.542	11.435	5.67	1.426	63.359	.186	
.126	15	12	.80	5.84	5.705	7.952	5.83	1.004	45.366	.133	
.128	9	6	.67	5.43	5.869	4.332	5.35	.553	25.424	1.149	

SILICA.10200

A

MAIN2
 ENTER THE P.D.F. CHOSEN: N
 ENTER FILE NAME: SILICA.10200
 FILE LIMITS ARE 1 3
 WHICH RECORD DO YOU WANT? 1
 NUMBER OF BINS TO BE GROUPED TOGETHER = 3

CRDV R-4197/81 (NON CLASSIFIÉ)

Bureau - Recherche et Développement, MDN, Canada.
CRDV, C.P. 8800, Courcellette, Qué. GOA 1R0

"Détermination du seuil d'endommagement de surfaces optiques par un laser CO₂ impulsional"
par J.C. Ancia et R.W. MacPherson

Nous décrivons une technique expérimentale permettant de déterminer le seuil d'endommagement des surfaces optiques de verre et de plastique irradiées par un laser CO₂ TEA impulsional. Les densités d'énergie correspondant à une probabilité d'endommagement de 50%, telles qu'estimées par une analyse probit, sont de 4.0 J/cm² pour la silice fondue, de 2.1 J/cm² pour le verre sodocalcique, de 2.3 J/cm² pour le thermoplastique, de 2.3 J/cm² pour le plastique acrylique et de 1.7 J/cm² pour le polystyrène. Nous présentons une interprétation des distributions statistiques observées en fonction de divers mécanismes d'endommagement. Enfin, plusieurs améliorations susceptibles d'accroître la précision des résultats obtenus sont suggérées. (NC)

CRDV R-4197/81 (NON CLASSIFIÉ)

Bureau - Recherche et Développement, MDN, Canada.
CRDV, C.P. 8800, Courcellette, Qué. GOA 1R0

"Détermination du seuil d'endommagement de surfaces optiques par un laser CO₂ impulsional"
par J.C. Ancia et R.W. MacPherson

Nous décrivons une technique expérimentale permettant de déterminer le seuil d'endommagement des surfaces optiques de verre et de plastique irradiées par un laser CO₂ TEA impulsional. Les densités d'énergie correspondant à une probabilité d'endommagement de 50%, telles qu'estimées par une analyse probit, sont de 4.0 J/cm² pour la silice fondue, de 2.1 J/cm² pour le verre sodocalcique, de 2.3 J/cm² pour le thermoplastique, de 2.3 J/cm² pour le plastique acrylique et de 1.7 J/cm² pour le polystyrène. Nous présentons une interprétation des distributions statistiques observées en fonction de divers mécanismes d'endommagement. Enfin, plusieurs améliorations susceptibles d'accroître la précision des résultats obtenus sont suggérées. (NC)

CRDV R-4197/81 (NON CLASSIFIÉ)

Bureau - Recherche et Développement, MDN, Canada.
CRDV, C.P. 8800, Courcellette, Qué. GOA 1R0

"Détermination du seuil d'endommagement de surfaces optiques par un laser CO₂ impulsional"
par J.C. Ancia et R.W. MacPherson

Nous décrivons une technique expérimentale permettant de déterminer le seuil d'endommagement des surfaces optiques de verre et de plastique irradiées par un laser CO₂ TEA impulsional. Les densités d'énergie correspondant à une probabilité d'endommagement de 50%, telles qu'estimées par une analyse probit, sont de 4.0 J/cm² pour la silice fondue, de 2.1 J/cm² pour le verre sodocalcique, de 2.3 J/cm² pour le thermoplastique, de 2.3 J/cm² pour le plastique acrylique et de 1.7 J/cm² pour le polystyrène. Nous présentons une interprétation des distributions statistiques observées en fonction de divers mécanismes d'endommagement. Enfin, plusieurs améliorations susceptibles d'accroître la précision des résultats obtenus sont suggérées. (NC)

CRDV R-4197/81 (NON CLASSIFIÉ)

Bureau - Recherche et Développement, MDN, Canada.
CRDV, C.P. 8800, Courcellette, Qué. GOA 1R0

"Détermination du seuil d'endommagement de surfaces optiques par un laser CO₂ impulsional"
par J.C. Ancia et R.W. MacPherson

Nous décrivons une technique expérimentale permettant de déterminer le seuil d'endommagement des surfaces optiques de verre et de plastique irradiées par un laser CO₂ TEA impulsional. Les densités d'énergie correspondant à une probabilité d'endommagement de 50%, telles qu'estimées par une analyse probit, sont de 4.0 J/cm² pour la silice fondue, de 2.1 J/cm² pour le verre sodocalcique, de 2.3 J/cm² pour le thermoplastique, de 2.3 J/cm² pour le plastique acrylique et de 1.7 J/cm² pour le polystyrène. Nous présentons une interprétation des distributions statistiques observées en fonction de divers mécanismes d'endommagement. Enfin, plusieurs améliorations susceptibles d'accroître la précision des résultats obtenus sont suggérées. (NC)

CRDV R-4197/81 (NON CLASSIFIÉ)

Bureau - Recherche et Développement, MDN, Canada.
CRDV, C.P. 8800, Courcellette, Qué. GOA 1R0

"Détermination du seuil d'endommagement de surfaces optiques par un laser CO₂ impulsional"
par J.C. Ancia et R.W. MacPherson

Nous décrivons une technique expérimentale permettant de déterminer le seuil d'endommagement des surfaces optiques de verre et de plastique irradiées par un laser CO₂ TEA impulsional. Les densités d'énergie correspondant à une probabilité d'endommagement de 50%, telles qu'estimées par une analyse probit, sont de 4.0 J/cm² pour la silice fondue, de 2.1 J/cm² pour le verre sodocalcique, de 2.3 J/cm² pour le thermoplastique, de 2.3 J/cm² pour le plastique acrylique et de 1.7 J/cm² pour le polystyrène. Nous présentons une interprétation des distributions statistiques observées en fonction de divers mécanismes d'endommagement. Enfin, plusieurs améliorations susceptibles d'accroître la précision des résultats obtenus sont suggérées. (NC)

DREV R-4197/81 (UNCLASSIFIED)

Research and Development Branch, DND, Canada.
DREV, P.O. Box 8800, Courclette, Que. G0A 1R0
"Determination of Pulsed CO₂ Laser
Damage Thresholds of Optical Surfaces"
by J.C. Antil and R.W. MacPherson

An experimental technique is described for determining the damage thresholds of glass and plastic optical material surfaces, opaque to laser radiations, when irradiated with a pulsed TEA-CO₂ laser. Use of a probit analysis to estimate the irradiance required for a 50% probability of damage gives threshold levels of 4.0 J/cm² for fused silica, 2.1 J/cm² for soda-lime glass, 2.3 J/cm² for polycarbonate, 2.3 J/cm² for acrylic and 1.7 J/cm² for polystyrene plastics. The significance of the statistical distributions observed in attributing various mechanisms to the damage is discussed. Finally, some improvements are suggested to make the measurements more accurate. (U)

DREV R-4197/81 (UNCLASSIFIED)

Research and Development Branch, DND, Canada.
DREV, P.O. Box 8800, Courclette, Que. G0A 1R0
"Determination of Pulsed CO₂ Laser
Damage Thresholds of Optical Surfaces"
by J.C. Antil and R.W. MacPherson

An experimental technique is described for determining the damage thresholds of glass and plastic optical material surfaces, opaque to laser radiations, when irradiated with a pulsed TEA-CO₂ laser. Use of a probit analysis to estimate the irradiance required for a 50% probability of damage gives threshold levels of 4.0 J/cm² for fused silica, 2.1 J/cm² for soda-lime glass, 2.3 J/cm² for polycarbonate, 2.3 J/cm² for acrylic and 1.7 J/cm² for polystyrene plastics. The significance of the statistical distributions observed in attributing various mechanisms to the damage is discussed. Finally, some improvements are suggested to make the measurements more accurate. (U)

DREV R-4197/81 (UNCLASSIFIED)

Research and Development Branch, DND, Canada.
DREV, P.O. Box 8800, Courclette, Que. G0A 1R0
"Determination of Pulsed CO₂ Laser
Damage Thresholds of Optical Surfaces"
by J.C. Antil and R.W. MacPherson

An experimental technique is described for determining the damage thresholds of glass and plastic optical material surfaces, opaque to laser radiations, when irradiated with a pulsed TEA-CO₂ laser. Use of a probit analysis to estimate the irradiance required for a 50% probability of damage gives threshold levels of 4.0 J/cm² for fused silica, 2.1 J/cm² for soda-lime glass, 2.3 J/cm² for polycarbonate, 2.3 J/cm² for acrylic and 1.7 J/cm² for polystyrene plastics. The significance of the statistical distributions observed in attributing various mechanisms to the damage is discussed. Finally, some improvements are suggested to make the measurements more accurate. (U)

DREV R-4197/81 (UNCLASSIFIED)

Research and Development Branch, DND, Canada.
DREV, P.O. Box 8800, Courclette, Que. G0A 1R0
"Determination of Pulsed CO₂ Laser
Damage Thresholds of Optical Surfaces"
by J.C. Antil and R.W. MacPherson

An experimental technique is described for determining the damage thresholds of glass and plastic optical material surfaces, opaque to laser radiations, when irradiated with a pulsed TEA-CO₂ laser. Use of a probit analysis to estimate the irradiance required for a 50% probability of damage gives threshold levels of 4.0 J/cm² for fused silica, 2.1 J/cm² for soda-lime glass, 2.3 J/cm² for polycarbonate, 2.3 J/cm² for acrylic and 1.7 J/cm² for polystyrene plastics. The significance of the statistical distributions observed in attributing various mechanisms to the damage is discussed. Finally, some improvements are suggested to make the measurements more accurate. (U)